*Q. J. R. Meteorol. Soc.* (2003), **129**, pp. 1491–1511 doi: 10.1256/qj.01.189

# The Iberian Peninsula thermal low

By KLAUS P. HOINKA[1]* and MANUEL DE CASTRO[2]

[1]*Institut für Physik der Atmosphäre, DLR, Oberpfaffenhofen, Germany*
[2]*Dpto. Ciencias Ambientales, Universidad Castilla-La Mancha, Toledo, Spain*

(Received 9 November 2001; revised 26 September 2002)

SUMMARY

Statistics of the thermal low above the Iberian Peninsula are presented for the period between 1979 and 1993, based on gridded data from the European Centre for Medium-Range Weather Forecasts reanalysis project. The sample of days with a thermal low above the Iberian Peninsula was selected objectively using criteria applied to mean-sea-level pressure and 925 hPa geopotential fields. The synoptic- and regional-scale horizontal structure is characterized by the climatology of the 500 hPa geopotential and mean-sea-level pressure distributions. The diurnal evolution of the mean-sea-level pressure is portrayed by mean fields at 00, 06, 12 and 18 UTC. The climatological vertical structure of the thermal low is shown by relation to meridional and zonal cross-sections passing through the thermal low's centre. The diurnal evolution of the divergence, relative vorticity, potential temperature and vertical velocity is investigated. Statistics are presented also for the monthly frequency, geographical location, vertical extent and intensity of the Iberian thermal low.

KEYWORDS: ERA data Heated low

## 1. INTRODUCTION

A thermal low is a warm, shallow, non-frontal depression which forms above continental regions, mostly in the subtropics, but also in the lower midlatitudes. They form mostly during summer months because of the intense surface heating over land. The main areas of occurrence are regions with arid or semi-arid surfaces where there is little surface evaporation. Some thermal lows remain quasi-stationary above the regions of origin, reaching their maximum intensity during the afternoon followed by a substantial weakening during the night. Other thermal lows, for example the West Australian heat trough, may become mobile during the day and the intensity does not diminish overnight. The basic physical process responsible for generating a thermal low is the vertical expansion of the lowermost layers of the atmosphere due to convective heating, which produces divergence above these layers. The divergence aloft results in a lowering of the surface pressure.

Although regions where they are usually generated form a considerable portion of the earth's land surface, thermal lows have received comparatively little study. One reason might be that there is usually little difficulty in forecasting their occurrence. However, there are exceptions in various geographical region. The position of the western Australian trough is sometimes hard to forecast (Leslie 1980). Rácz and Smith (1999) emphasized that the occurrence of heat lows above Australia play an important role in modifying dry cold fronts which cross the continent. These cold fronts undergo a large diurnal variation in intensity which is forced by the presence of a thermal low. Thermal lows which form in the north-east of India and Pakistan contribute greatly to the summer monsoon (Ramage 1971; Chang 1972). Similarly, Leslie (1980) related Australian thermal lows to the summer monsoon. Blake *et al.* (1983) and Smith (1986a) studied the influence of the Arabian thermal low on the moisture advection towards the south-western part of the Arabian Peninsula which is affected by monsoon rain. Junning *et al.* (1986) analysed climatological factors which favour the development of thermal lows above the Qinghai-Xizang plateau in China and which induce the major part of the summer rain in this area. Another region with thermal lows is northern Africa (Griffiths

* Corresponding author: Institut für Physik der Atmosphäre, DLR, Postfach 1116, D-82230 Wessling, Germany.

and Soliman 1972) where the extreme surface aridity does not allow the formation of rain. Further areas characterized by thermal lows are Tasmania (Whitehead 1981) and the south-western United States (Rowson and Colucci 1992) where heat lows might induce local storms above mountainous regions.

Because thermal lows occur frequently above the Iberian Peninsula (henceforth denoted by IP) during summer, they are classified as one of the important weather types in the Iberian climatology (Linés 1970; Font 1983). Typically, shallow convection forms in the low, but precipitation does not occur. Nevertheless, strong pressure gradients occur at the periphery of the low and these cause low-level winds to blow from the coastal zones towards the interior of the peninsula. This can be seen in the trajectories of emissions which leave tall chimneys and spread diffusively (Millán *et al.* 1991). The Iberian thermal low is thought to be the most prominent example of its type in Europe. Nevertheless, similar but less intense thermal troughs have been observed also at higher latitudes in Europe. Scherhag (1936) determined the local diurnal pressure changes between morning (07 UTC) and afternoon (18 UTC) over Europe for a summer month. He showed that there is a mean diurnal pressure decrease of 4 hPa above the IP, about 3 hPa above the Alps and even 1 hPa above England. A similar circulation system is thermally forced over the Alps owing to the unequal heating of the atmosphere above the mountains and within the valleys and over the surrounding plains. From serial pilot balloon observations, Burger and Ekhart (1937) showed that there is a low-level inflow towards the centre of the Alps whereas divergence occurs at a height of about 5 km. The horizontal extent of the Alpine wind system was estimated to be about 150 km away from the main Alpine ridge.

In order to analyse regional characteristics that primarily influence the formation of summer thermal lows, Gaertner *et al.* (1993) performed a numerical study using a two-dimensional numerical model. They showed that the most prominent factors determining the intensity of thermal lows are the surface aridity during summer and the elevated height of the central Iberian plateau. Later, Portela and Castro (1996) simulated the thermal low with a high-resolution mesoscale model corroborating that surface winds blow inland as the low intensifies. These winds can increase in speed to more than 10 m $s^{-1}$ in particular areas as a result of a channelling effect, e.g. in river valleys and mountain passes. This effect might be of considerable relevance for choosing sites for the installation of wind-power stations. Alonso *et al.* (1994) emphasized the importance of friction and diabatic heating on the resulting potential-vorticity patterns associated with the Iberian thermal low. Millán *et al.* (1991) found that the thermal convection transports photochemically contaminated particles into the stably stratified layer where they could be advected over large distances. Gaertner *et al.* (2001) showed that convergence of maritime air reinforced by thermal lows could make a significant contribution to the local water balance over the mountainous north-eastern periphery of the IP during summer.

All textbooks on climatology of the IP weather (e.g. Linés 1970) mention that the thermal low is a prominent weather during summer, but none of these studies provide a climatology of this phenomenon. Portela and Castro (1991) made a first approach by using three-hourly mean surface pressures taken at 82 synoptic stations located in Spain and Portugal for a period of nine non-consecutive years (1973–1977 and 1985–1988). Applying an objective analysis method they determined the monthly frequency of thermal lows and classified them by their intensity. They showed that the months with the most days with thermal lows are July and August with an average of more than 60%. Portela and Castro (1996) recently analysed the vertical structure, horizontal extent and the likely location of occurrence of the Iberian thermal low using analysis data

provided by the European Centre for Medium-Range Weather Forecasts (ECMWF). However, their statistics represent a relatively short four-year period (1985–1988) and their database cannot be considered to be homogeneous because there were changes in the ECMWF analysis and forecasting system during that period. The present paper considers a longer period of 15 years (1979–1993) using data provided by the ECMWF ReAnalysis Project (ERA). This dataset was created by rerunning a selected model version with its analysis cycle for the whole period (Gibson *et al.* 1997).

Usually the characteristics of a thermal low are described in terms of mean-sea-level pressure (MSLP). Yet it is not clear how to interpret pressure in terms of dynamics, whereas relative vorticity can be easily related to dynamical processes. Rácz and Smith (1999) have shown that the low-level relative vorticity in thermal lows is significantly out of phase with the pressure field. However, their idealized simulation did not consider the impact of orography and they assumed that the thermal low was embedded into an undisturbed environment. Therefore, we explore here how the thermal low's vorticity structure in the idealized simulations compares with observed flow situations.

The purpose of the present study is to determine a climatology of the thermal low above the IP objectively, based on data covering many years. The mean diurnal evolution is determined together with the horizontal and vertical structure of lows. The statistics of the climatology presented extend those given by Portela and Castro (1996). These statistics represent the characteristics of the thermal low better because they are derived for a much longer period of time and are based on a homogeneous time series of analysis data. The climatology of thermal-low days above the IP given here represents an important part of the present-day climatic state of the IP. Sufficient knowledge of the present-day climatic state, characterized by appropriate statistics such as the frequency, intensity and location of the Iberian thermal low, is necessary for the detection of a possible climatic change for the IP.

Data and criteria are described in section 2. The following section discusses statistics of the frequency of the occurrence, of the location of the Iberian thermal low's centre, and of its intensity. This is followed by a presentation of the horizontal mean fields of the surface pressure and of the 500 hPa surface height. Then, zonal and meridional cross-sections above the IP are presented to show the climatological structure of the troposphere for days with thermal lows.

## 2. Data and criteria

The present study considers a data sample of 15 years from 1979 to 1993. The ECMWF supplies the so-called 'ERA-data' in two subsets that were used here: standard pressure-level data (15 levels). The analysis scheme applied in the ERA project is based on the T106 spectral truncation, which corresponds with a resolution of about 1.125° in latitude and longitude. For the present study the data were interpolated to a finer grid with 0.5° in latitude and longitude.

In an earlier study, Portela and Castro (1991) used the observed surface-station pressure to separate days with a thermal low from those without, as well as to determine characteristics of the thermal lows. The disadvantage of this dataset is that the observations are unequally distributed over the IP. In later work, Portela and Castro (1996) used the MSLP. Since the mean height of the IP is approximately 600 m (Lautensach 1964), the MSLP is determined from an extrapolation for a layer of considerable depth at most grid points raising questions about the accuracy of the horizontally analysed pressure fields. We have found that horizontal pressure differences depend sensitively on the quality of the vertical interpolation. Early observations of the IP thermal low were

questioned because of the problems of reducing station pressure data to sea-level pressure. The mean surface height of the IP is at about the same height as the 925 hPa surface for which observed pressure and temperature measurements are used to determine the corresponding ERA level data. Therefore, in contrast to earlier studies, we use the height of the 925 hPa surface instead of the MSLP, because it provides a better representation of the observations. The height of the 925 hPa surface is used for criteria which need horizontal differences whereas the MSLP is used also for criteria which involve absolute values.

The basic task is to separate thermal lows from synoptic-scale lows entering the IP from the Atlantic ocean. Synoptic charts show that the minimum pressure in Iberian thermal lows is not less than 1004 hPa. These lows are mesoscale systems which develop in an anticyclonic environment. Because there is no surface low at 06 UTC, the anticyclone at this time dominates the low-level pressure pattern and the surface pressure above north-western Spain is larger or at least close to its normal value of 1012 hPa. Therefore, a threshold value of 1011 hPa was chosen for our criterion. Because the Iberian thermal low disappears during the night, but the Saharan one does not, a further criterion eliminates all days during which the Iberian and Saharan depressions are indistinguishable. This linking becomes obvious in the south-east of the IP, the area which is closest to Africa. A further fact is that the thermal lows are of continental character with lower pressure above the land mass and a higher one above the surrounding sea. In order to validate the selected criteria, three years were checked by means of daily comparisons with surface and upper-air charts published by the Spanish Meteteorological Office. None of the thermal-low days selected within this period corresponded to a baroclinic low. Therefore we are confident that the selected lows are generated thermally by surface heating. On the other hand not all Iberian thermal lows were selected, particularly those that were not totally surrounded by higher pressure.

Following Portela and Castro (1996), 18 UTC is considered to be the time of the significant pressure minimum because the thermal-low pattern is more pronounced than at 12 UTC. The following criteria, which have been adapted from those proposed by Portela and Castro (1991), are considered to separate days with and without thermal low above the IP.

(i) At 06 and 18 UTC, the MSLP above the IP (Fig. 1, area A) must be larger than 1002 hPa allowing one grid-point failure.
(ii) At 06 UTC the grid-point-averaged MSLP must be greater than 1011 hPa at the northern and north-western rim of the IP (Fig. 1, squares in region NW and N).
(iii) At 18 UTC, the minimum height of the 925 hPa surface must be located above the IP (Fig. 1, area A) considering all grid-point data within an area bounded by 13°W, 7°E, 33°N and 46°N.
(iv) The grid-point-averaged MSLP tendency between 06 and 18 UTC must be negative in the south-eastern corner of the IP (Fig. 1, triangles in region SE).
(v) At 18 UTC, the grid-point-averaged height of the 925 hPa surface above the interior area (triangles) must be less or at least equal to that of the peripheral area (squares) within all considered regions separately (NW, N, etc.).

We show here for the first time zonal and meridional vertical cross-sections of potential temperature, vertical velocity, relative vorticity and divergence traversing the Iberian thermal low. The location of the cross-sections are chosen in relation to the most likely region of the thermal-low centres which was determined in a first step (see section 3). These cross-sections are obtained by averaging the data over all July days

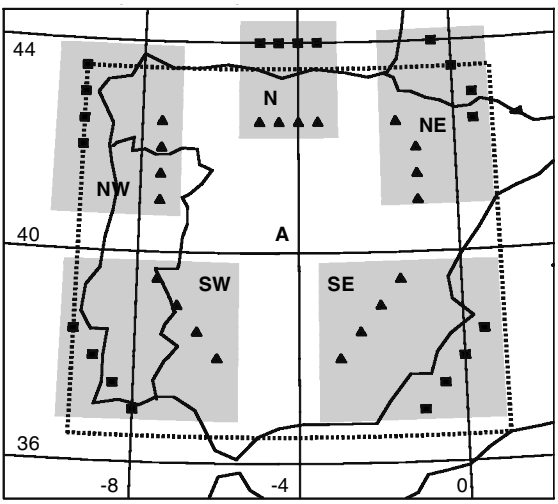


Figure 1. Scheme of criteria as described in section 2. Criteria (i) and (iii) are applied within region A (limited by the dotted line). The shaded areas (NW, N, NE, SE and SW) indicate the regions where differences in the averaged grid-point values between the interior (triangles) and peripheral (squares) areas are calculated for criteria (v).

with a heated low for the period 1979 to 1993. The meridional cross-section covers the region between 33°N and 46°N along the meridian of 4°W and the zonal section extends from 13°W to 7°E along the parallel of latitude 40.5°N. Following Portela and Castro (1996), the intensity is determined as positive anomaly from the MSLP averaged over a selected area and also as its standard deviation. The average considers all grid-point values within the area of $\pm 1.5°$ in latitude and longitude around the pressure minimum; this area extends approximately 300 km in both longitudinal and latitudinal direction. The vertical extent of the thermal low is determined by considering the change of sign in the vertical profiles of divergence, vorticity and the Laplacian of potential temperature above the thermal low's centre. Another parameter of interest would be the horizontal extent of the thermal low. However, there is no reasonable measure of this quantity; therefore, statistics on this cannot be presented here.

## 3. Frequency of occurrence

Table 1 lists the monthly mean number of days with a thermal low above the IP throughout the year. During the peak months of July and August, thermal lows were observed on about 45% of the days. The pre-peak season (May and June) shows a higher frequency of occurrence (14% and 34%) than the post-peak months of September and October (18% and 2%). A similar annual variability was reported by Portela and Castro (1996). Rowson and Colucci (1992) found a similar annual variation for the south-western United States, the peak month there being July with slightly fewer events in August. However, the frequencies were significantly larger, for example about 81% in July. Even during the winter months, December and January, frequencies of occurrence of about 3% were found. The reason for this is presumably because the area is subtropical. Whitehead (1981) showed that thermal lows occur in Tasmania during the southern hemisphere summer. The peak months of occurrence are December and January, with frequencies of up to 73%. In general about 42% of the days per month are observed to have thermal lows during summer whereas this frequency reduces to about

TABLE 1. STATISTICS OF IBERIAN THERMAL LOWS (1979–1993)

| Period | All days | Days per month | % of days |
|---|---|---|---|
| JAN | 0 | 0.0 | 0.0 |
| FEB | 3 | 0.2 | 0.1 |
| MAR | 13 | 0.9 | 2.9 |
| APR | 15 | 1.0 | 3.3 |
| MAY | 65 | 4.3 | 13.9 |
| JUN | 151 | 10.1 | 33.7 |
| JUL | 212 | 14.1 | 45.5 |
| AUG | 210 | 14.0 | 45.2 |
| SEP | 81 | 5.4 | 18.0 |
| OCT | 11 | 0.7 | 2.3 |
| NOV | 1 | 0.1 | 0.3 |
| DEC | 0 | 0.0 | 0.0 |
| Spring | 93 | 2.1 | 6.7 |
| Summer | 573 | 12.7 | 41.5 |
| Autumn | 93 | 2.1 | 6.8 |
| Winter | 3 | 3.0 | 0.0 |
| 1979–1993 | 762 | 4.2 | 13.9 |

7% during spring and autumn. There is also a moderate year-to-year variability ranging from 26% to 61% for July and 16% to 64% for August. From the time series a trend is not obvious in the mean annual number of thermal-low days. During the entire period from 1979 until 1993, thermal lows were found on 762 days. About 14% of the entire period can be classified as having thermal-low events.

Statistics of western Mediterranean cyclones (Campins *et al.* 2000) showed that about 40 cyclones occurred above the central IP during the summer months from 1992 to 1995. Because this number refers to cyclones located within the area ($2^\circ \times 2^\circ$) for several consecutive days, the number of days with cyclones is probably larger. This number contains thermal lows as well as cyclones, the latter occurring rarely in summertime above the IP. Thus the number given in Table 1 is consistent with the frequency found by Campins *et al.* (2000). Other statistical studies indicate a lower frequency: for example Soler and Hernandez (1977) found about 8% annually and 22% for summer. In order to show the relative importance of the weather type 'thermal low' for the IP, relevant numbers of other types are given by the annual percentage of days: 10% with a cold front encountered above the entire peninsula (Hoinka and Seco 1991); 10% with a cyclonic event associated with precipitation (Soler and Hernandez 1977); and 2% of cut-off lows (Hernandez 1997).

In order to determine the probable location of the Iberian thermal low, the percentage frequencies of its location were calculated for two samples: the entire sample of 762 cases (Fig. 2(a), ALL) and the sample of the 212 July events (Fig. 2(b), JUL). In both cases the most likely region of the thermal low is at about 40.5°N and 4.0°W with a maximum of more than 6% (for ALL) which represents 48 cases at the central grid point. About 50% of all events were located in a small region of radius 0.75° latitude and longitude around the mean centre. For July these numbers result in 6.1% (13 events) and 58.3% (124 events). Thus the variability in location of the low's centre is smaller in July than during the entire period from February to November, i.e. the centres of most thermal lows are concentrated in a smaller area in July than in other months.

As shown by Wang (1987), different types of analyses, e.g. subjective and objective ones, might result in different locations of thermal-low centres. For example, Portela

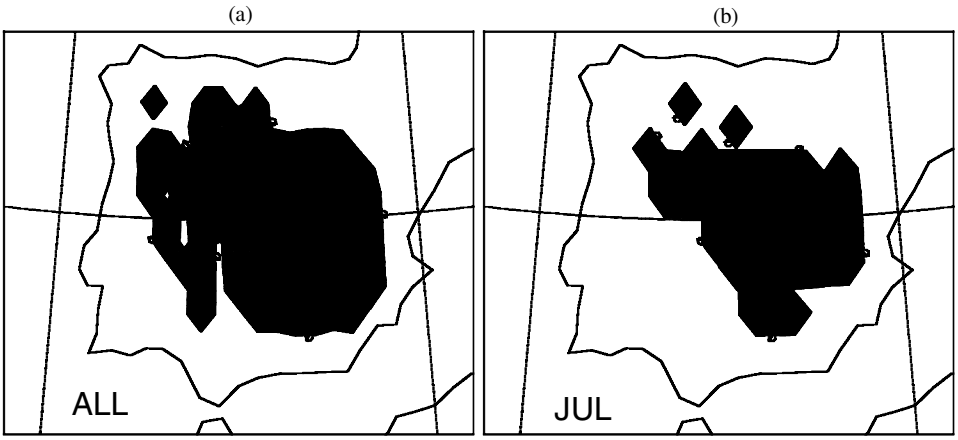


Figure 2. Frequency (%) of location of thermal-low centres determined for the period 1979–1993, 18 UTC: (a) all days (ALL) and (b) all days in July (JUL). Contour interval is 1%.

and Castro (1996) determined a slightly different climatological location of the thermal-low centre occurring at about 39.0°N and 6.0°W. In their study the low centre was located within a 0.75° radius of this location for 52% of all events. Their results are based on a sample of four years. Their database and criteria were different to those of the present study, which may explain the different geographical distribution of the low centres. A further reason for the northward shift of the thermal low's averaged location might be the fact that the smoothed ERA orography places the main orography above the IP at about 41.4°N and 3.3°W. However, had we used MSLP or the 1000 hPa surface instead of the 925 hPa surface, the influence of the orographic smoothing might have been more important.

Various quantities have been used to characterize the vertical extent of thermal lows: for example Blake *et al.* (1983) used divergence, Wang (1987) used vorticity and Alonso *et al.* (1994) used potential vorticity. A characteristic property of the vertical thermodynamic structure of the thermal low is a deep mixed layer above the low's centre. At the surface there are strong horizontal gradients of potential temperature $\theta$ extending from the low's centre, but these gradients diminish with height. Therefore, the vertical profile of the Laplacian of potential temperature, $\nabla^2\theta$, can be used also as a measure for the depth of the low. In the present study we have averaged all vertical profiles taken above the centre of the low. The resulting averaged profile gives the mean structure above the low's centre relative to the land surface.

Figure 3 shows the mean profiles of divergence (div), vorticity (vort), and $\nabla^2\theta$ (LP-TH) at 18 UTC. Strong convergence occurs within a 1500 m deep surface-based layer above which there is a deeper layer of divergence extending to between 4 and 5 km. The level of non-divergence is between 2400 and 2500 m above mean-sea-level (amsl). The absolute values are larger for the surface layer than for the layer above it. Much larger depths (up to 4000 m) were found for the Tibetan Plateau (Wang 1987). The magnitude of $\nabla^2\theta$ is significantly larger in the well-mixed layer than above it, indicating that the thermal structure is disturbed only up to 3 to 4 km amsl. Finally, positive vorticity exists up to a height of about 2600 m above ground level (agl). In idealized numerical calculations, Rácz and Smith (1999) showed that the low-level relative vorticity is significantly out of phase with the pressure field and the maximum low-level vorticity occurs in the early morning hours, a finding that is supported by

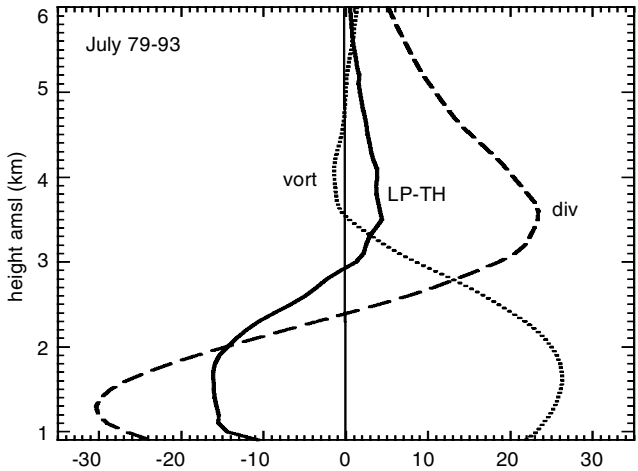


Figure 3. Mean vertical profiles of divergence (div; $10^{-6}$ $s^{-1}$), vorticity (vort; $10^{-6}$ $s^{-1}$), and Laplacian of potential temperature (LP-TH; $10^{-11}$ K $s^{-2}$) above the thermal-low centre at 18 UTC. The averaging sample contains all thermal lows of July 1979–1993.

TABLE 2. STATISTICS OF THE VERTICAL EXTENT (m amsl) OF THE IBERIAN THERMAL LOWS AT 18 UTC (1979–1993)

| | | Laplacian of $\theta$ | | Divergence | |
|---|---|---|---|---|---|
| Period | Sample | Mean | Std dev | Mean | Std dev |
| MAR | 13 | 2343 | 1293 | 2256 | 955 |
| APR | 15 | 2782 | 448 | 2292 | 202 |
| MAY | 65 | 2849 | 555 | 2196 | 344 |
| JUN | 151 | 2809 | 511 | 2347 | 300 |
| JUL | 212 | 2950 | 621 | 2383 | 286 |
| AUG | 210 | 2887 | 501 | 2360 | 273 |
| SEP | 81 | 2726 | 524 | 2190 | 228 |
| OCT | 11 | 2177 | 877 | 1968 | 368 |
| 1979–1993 | 762 | 2846 | 585 | 2312 | 318 |

observations of frontal troughs over northern Australia (Smith *et al.* 1995). In addition, Wang (1987) indicated that within a thermal low the areas with maximum vorticity and divergence do not coincide. He showed that the vorticity centre is shifted by about 100 km to the west of the divergence centre. It follows that the vertical profile of relative vorticity at 18 UTC is not an appropriate measure for the depth of the thermal low.

Table 2 lists the annual variation of the thermal low's vertical extent as obtained from the change of sign in the corresponding vertical profiles of $\nabla^2\theta$ and divergence. Due to the fact that the maximum value of the ERA orography above the IP is around 800 m, the lowest usable level for horizontal derivatives, e.g. $\nabla^2\theta$, is at that height. The maximum depth of the low is observed during July when the thermal lows are strongest: 2150 m agl for $\nabla^2\theta$ and 1580 m for divergence. The annual variation of the vertical extent is between 400 m for divergence and 800 m for $\nabla^2\theta$. Usually the level of non-divergence is found below 700 hPa. However, for continental regions with substantial surface heating the mixed layer might extend up to a pressure level of 550 hPa, as observed in the Arabian Peninsula (Smith 1986b).

TABLE 3. STATISTICS OF THE IBERIAN THERMAL-LOW INTENSITY (hPa) AT 18 UTC (1979–1993). INTENSITY IS DETERMINED AS POSITIVE ANOMALY FROM THE AVERAGED MEAN-SEA-LEVEL PRESSURE (A) AND AS ITS STANDARD DEVIATION (B).

| Period | Sample | A Mean | A Std dev | B Mean | B Std dev |
|---|---|---|---|---|---|
| MAR | 13 | 0.53 | 0.19 | 0.51 | 0.14 |
| APR | 15 | 0.61 | 0.19 | 0.56 | 0.17 |
| MAY | 65 | 0.60 | 0.19 | 0.59 | 0.20 |
| JUN | 151 | 0.62 | 0.28 | 0.68 | 0.26 |
| JUL | 212 | 0.65 | 0.23 | 0.73 | 0.20 |
| AUG | 210 | 0.59 | 0.22 | 0.69 | 0.22 |
| SEP | 81 | 0.57 | 0.23 | 0.67 | 0.20 |
| OCT | 11 | 0.50 | 0.15 | 0.48 | 0.11 |
| 1979–1993 | 762 | 0.61 | 0.23 | 0.68 | 0.22 |

The depth can be used as a measure of intensity. On the other hand, it would be better to have an independent measure of intensity. As mentioned in section 2, the intensity is calculated as the anomaly of pressure from the mean pressure averaged over a defined limited area around the pressure centre. Table 3 shows the annual variation of the intensity of the thermal low. The positive anomalies from the MSLP and, as a second measure, the deviation from the mean pressure value are given for the chosen limited region around the pressure minimum. Again the maximum value occurs during July for both measures.

## 4. HORIZONTAL STRUCTURE

The size of the IP lies within the range normally considered to be mesoscale (Orlanski 1975), so that the thermal-low systems generated above the peninsula are mesoscale in size. Therefore, it is of interest to analyse the synoptic environment in which such mesoscale thermal systems develop. We consider only the months from May to September because the frequency of the thermal lows in the other months is very small—less than 4% (Table 1). Three types of fields are presented: data for days with thermal low (henceforth denoted by TL); for days without thermal low (NTL); and for the difference of both fields, TL minus NTL (DIF).

The mean MSLP for days with thermal lows at 18 UTC when the lows are well developed are shown in Figs. 4(a) and (d) for the months of May (late spring) and July (midsummer). Apparently the synoptic surface situation on days with a thermal low is similar for both months: an anticyclone over the Atlantic Ocean extends a ridge towards central Europe and the Mediterranean Sea. The isobars are deformed above the IP, where a small weak centre of low pressure appears at the surface. Moreover, strong gradients of MSLP occur along the western and northern edges of the IP.

The most notable differences between May and July appear in the averaged MSLP fields for days without thermal lows (Figs. 4(b) and (e)). The location of the anticyclone in May permits the entry of frontal troughs or extratropical cyclones from the Atlantic Ocean over the IP, which makes it impossible for the thermal lows to develop. In contrast, in July, the strong anticyclone does not favour the penetration of these disturbances. The averaged synoptic-scale environment for days without thermal lows (NTL, Fig. 4(e)) is very similar to that for the sample of all thermal low days (TL, Fig. 4(d)). It appears that in this case the pressure gradients at the northern and western boundaries of the IP are weaker than at its southern boundary, which might give the impression

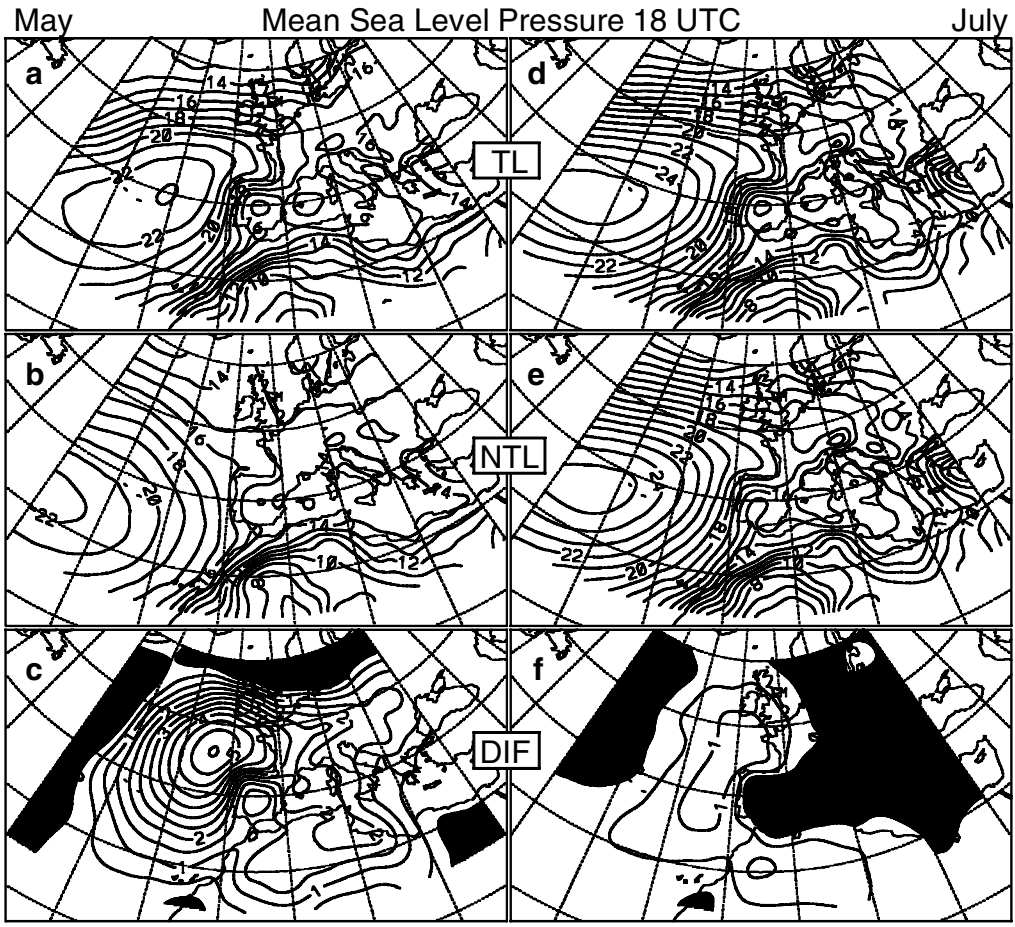


Figure 4. Deviations (hPa) of the mean-sea-level pressure from 1000 hPa for 18 UTC 1979–1993: (a)–(c) May and (d)–(f) July. (a) and (d) thermal low above the Iberian Peninsula (TL); (b) and (e) no thermal low (NTL); (c) and (f) difference (DIF) between TL and NTL. Shaded areas indicate negative deviations.

that the permanent thermal low above the Sahara extends across the interior of the IP. The weak differences between the two fields (TL and NTL) result from the fact that, in general, the Atlantic anticyclone influences the flow over the IP during most days in midsummer because episodes with intrusions of Atlantic perturbations are rare during this time of the year (Linés 1981).

Clearly, the difference in the synoptic environment of the mean July fields between the sample for days with and without thermal lows depends on the selection criteria related to the SE and SW rim. Thus, the related criteria (iv) and (v) (see section 2) are fulfilled as soon as the surface heating above the IP is strong enough to form a thermal low with sufficient intensity that MSLP gradients appear at the southern borders of the peninsula. In the case of weaker heating the resulting thermal low would be less intense, and thus in turn the corresponding MSLP gradients from north Africa towards the interior of the IP would change sign. This would lead to not all criteria being fulfilled. The cases with strongest heating correspond to the sample of days when the Atlantic anticyclone is more closely located over the peninsula, as can be seen in Fig. 4(f). This figure shows that there is a negative MSLP difference (thermal low more

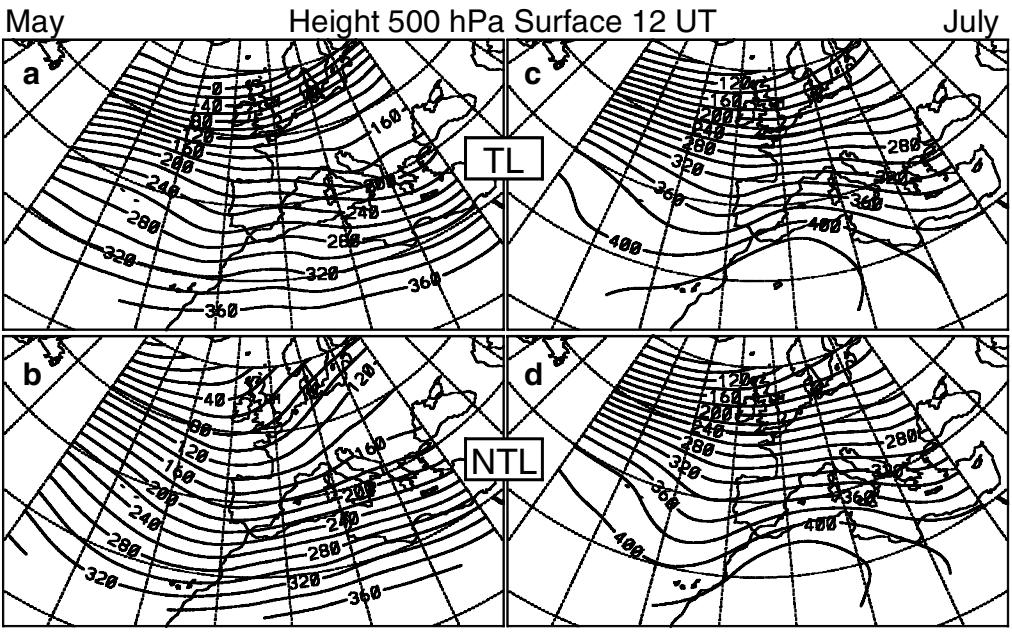


Figure 5. Deviations (m) of the 500 hPa surface height from 5500 m for 12 UTC 1979–1993: (a)–(b) May and (c)–(d) July. (a) and (c) thermal low above the Iberian Peninsula (TL); (b) and (d) no thermal low (NTL).

intense) in the centre of the peninsula as soon as there is a positive MSLP difference in the northern oceanic region and to the west of the IP.

A simple method for interpreting the differences apparent in Fig. 4 would be to consider synoptic-scale parameters in order to separate days with favourable and unfavourable synoptic-scale environment for allowing a thermal low to form. Thus, although days in July have a favourable, anticyclonic environment, the thermal low is separated from the low above northern Africa only on slightly fewer than half the days in the sample (45.5%). In May, however, there is a larger number of days with an unfavourable synoptic-scale environment (not anticyclonic) as can be seen in Fig. 4(c) where positive values of MSLP difference appear in the relative pressure minimum above the IP.

A similar interpretation would apply for explaining the mean structures at the 500 hPa surface at 12 UTC (Fig. 5). Again Figs. 5(a) and (c) show that the patterns of the mean contours for thermal-low days during May and July are similar, although the mean geopotential height is different. Above the west coast of the peninsula there is a small-amplitude short-wave trough embedded in the predominantly zonal flow. This pattern appears also in July for days without thermal lows and indicates the weak variability of the synoptic situation during midsummer. However, the mean May structure of days without thermal lows shows a deeper trough which is embedded in a zonal wave of larger wavelength above the western part of the IP. This indicates that the unfavourable synoptic situations for the formation of thermal lows are more frequent in May than in July.

It turns out that the mean synoptic-scale pattern at the surface as well as in the midtroposphere for days with thermal lows is similar for all months between May and September, although only the months of May and July have been presented here. The following comments are restricted to the July data. This is because the sample

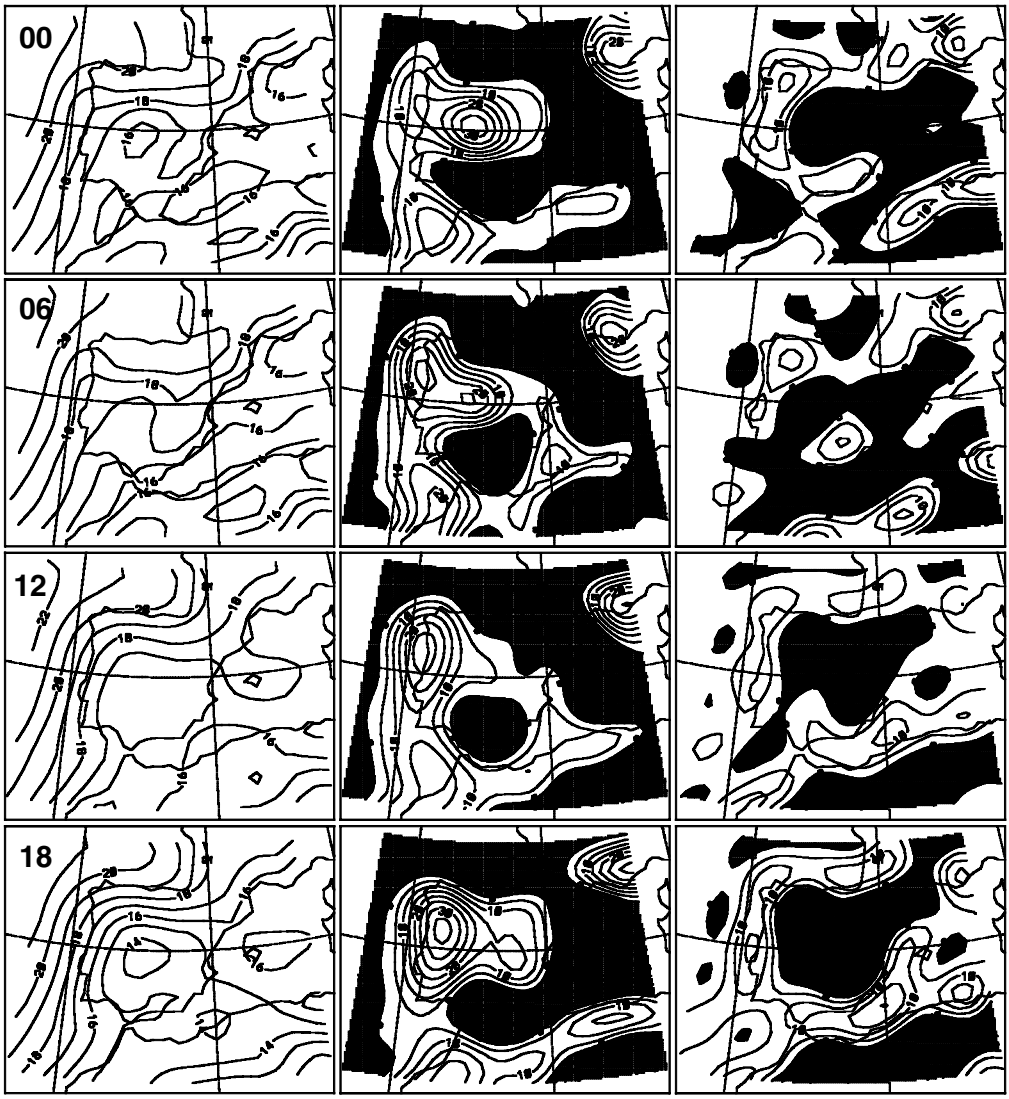


Figure 6. Deviations of the mean-sea-level pressure from 1000 hPa (left column) (hPa), relative vorticity (centre column) and divergence (right column) (both in $10^{-6}$ $s^{-1}$ at 925 hPa), at 00, 06, 12 and 18 UTC for thermal lows (July 1979–1993). The shaded areas indicate anticyclonic vorticity and convergence.

sizes for cases with and without a thermal low are about the same and also because the structure of thermal lows that occur during the other months of the year is similar, but the lows are less intense.

We consider now the mesoscale environment. Figure 6 shows the averaged MSLP, relative vorticity and divergence at 00, 06, 12 and 18 UTC for the sample of thermal-low days above the IP. The mean values are determined from all the relevant days for the period 1979 to 1993. We use the four available synoptic times to characterize the diurnal evolution. This is supported by the large number of thermal-low days during July forming the subsample (see Table 1) and by the fact that many members of this

subsample are parts of the time series of thermal lows that last for more than two consecutive days.

As expected for a thermally driven system, the maximum intensity, which refers here to the minimum MSLP, appears in the late afternoon, characterized here by the pressure field at 18 UTC. Of course, the peak intensity may occur a few hours earlier or later, the temporal resolution of the data being too coarse to be more precise. The work of Portela and Castro (1996), based on three-hourly surface observations, indicates that the peak hour is between 15 and 18 UTC which is corroborated by the numerical simulation of Gaertner *et al.* (1993). A characteristic of the Iberian thermal low is the moderate anisotropy in the radial horizontal gradients. It can be seen that during the peak phase of the evolution at 18 UTC the radial gradients are strongest—about 3 hPa per 100 km—towards the north and the west and weakest towards the south-east. The magnitude of this mesoscale horizontal pressure gradient at the surface is large. Similar sized surface-based pressure differences have been observed within other mesoscale circulation systems such as the Alpine Foehn (Hoinka and Rösler 1987).

During the night the thermal low weakens and finally disappears during the early morning around 06 UTC. Sometimes the net surface cooling begins before sunset. As a result, convection and thermal expansion within the mixed layer ceases, but mass divergence aloft and lower-layer convergence still go on for several hours. Therefore, the shallow thermal low progressively fills during the night.

The large MSLP gradients observed at the western and northern edge of the IP relate to the typical synoptic-scale structure of the MSLP field above the Azores during summer associated with a continental low above the Saharan desert. The weak horizontal MSLP gradients in the south-east of the IP indicates that in this area, the intense thermal low above the Sahara is united with the Iberian thermal low. The object of the present study is to select and consider only those Iberian thermal lows which are separate from the Saharan one. This is accomplished by applying criterion (iv) in the areas SE and SW (Fig. 1).

Using observational data it is possible to provide a preliminary analysis which is based on the MSLP tendencies between the four available times (00, 06, 12 and 18 UTC). This might help to establish that the rhythm of strengthening or weakening of the MSLP gradients is not isotropic above the entire IP. The strongest falling tendencies (up to 2.5 hPa per 6 h) are observed in the centre of the IP between 12 and 18 UTC, which coincides approximately with the climatological mean location of the thermal-low centre. The strongest rising tendencies (up to 2.5 hPa per 6 h) occur over the eastern part of the IP between 18 UTC and 00 UTC on the following day. At 00 UTC, the thermal-low centre is found in the same location as was observed during the peak hour, although the mean pressure is higher. Further to the east, a weak ridge of higher pressure is evident. This ridge can be found until 06 UTC (Fig. 6), but disappears rapidly by noon. There are two noteworthy facts that support the idea that the Saharan low does not influence the formation of the Iberian thermal low: (i) the smaller-scale Iberian thermal low decays more rapidly during the night than the stronger and larger Saharan depression, and (ii) the climatological centre of the Iberian thermal low is located close to the geographical centre of the IP. Nevertheless, one has to take into account that the climatological patterns shown in Fig. 6 are obtained by selecting only those days for which all criteria were fulfilled. In summary, the reduction in the daily MSLP caused by the surface heating in the central IP is strong enough to generate a pressure minimum which is 'isolated' from that of northern Africa.

Rácz and Smith (1999) performed an idealized numerical simulation of a thermal low located within an undisturbed environment in the absence of orography. They found

that the thermal low undergoes a strong diurnal cycle, not only in MSLP, but also in the relative vorticity. They found also that the minimum in relative vorticity occurs at 03 h local time, some 10 h later than the minimum MSLP. Using the same model with a plateau-type orography, Reichmann and Smith (2003) showed that the mixed layer becomes deeper than without orography. The vertical velocity in the centre of the heat low is weaker when the plateau is surrounded by sea than when it is not. How do these idealized situations relate to reality, where both synoptic-scale environment and orography are present? The ERA data show that the low-level relative vorticity is not only related to the formation of the thermal low. Between 06 and 18 UTC, the centre of the maximum cyclonic (positive) relative vorticity is found above the west coast of the IP. This is because of broad-scale horizontal wind shear associated with northerly winds along the Portuguese coast, which are frequently observed during summertime anticyclonic situations. At the same time an anticyclonic (negative) vorticity centre exists above the Strait of Gibraltar, which is also related to horizontal wind shear frequently associated with strong easterly winds. At 00 UTC the cyclonic vorticity centre moves towards the interior of the IP. Thus, there is a phase shift between the minimum MSLP and the maximum cyclonic vorticity of about 6 h. This finding is in accordance with idealized numerical model calculations (Rácz and Smith 1999). In contrast to these simulations the observations show an irregular distribution of vorticity due to the complicated shape of the Iberian orography and to regional characteristics such as strong winds blowing parallel to the western and southern coast of the IP. Accordingly, it is difficult to interpret the observed relative-vorticity fields because of their irregular structure.

## 5. Vertical structure

The vertical structure above a thermal low is usually shown by vertical cross-sections intersecting the thermal low. Wang (1987) showed such cross-sections in certain case-studies, but we are not aware of published cross-sections of climatological fields. Figure 7 shows zonal and meridional cross-sections of divergence which pass through the climatological centre of the thermal low, which is located at 40.5°N and 4°W. The figure shows fields for 00, 06, 12 and 18 UTC averaged over all thermal-low days of July during 1979–1993.

A zone of maximum convergence is found close to the surface, underlying a layer of divergence. This dipole structure is strongest at 18 UTC and persists until 00 UTC, but its depth decreases with time. At the peak intensity of the low, the convergence attains a magnitude exceeding $3 \times 10^{-5}$ s$^{-1}$. This is stronger than the values observed above the Tibetan Plateau (Wang 1987), which were typically $1 \times 10^{-5}$ s$^{-1}$. Another characteristic feature is that there exists an asymmetry in the dipole. The convergence layer towards the west is shallower and the divergence layer reaches the surface close to the Atlantic coast. To the east of the centre, however, the divergence layer is elevated above the ground at all times. At 18 UTC the upper divergence zone approaches the surface-based divergence zone above the Mediterranean coast. The zonal asymmetry is a result of the existing synoptic-scale convergence above the eastern IP which is present for the entire day. A similar pattern appears in the meridional cross-section. In this case divergence occurs down to the surface in the southern part of the IP, although not in the northern part. There is a secondary maximum in the convergence which is located above the coast of Cantabria. The fact that the divergence zone spreads out to the surface in the area between the IP and northern Africa at all hours of the day indicates that the

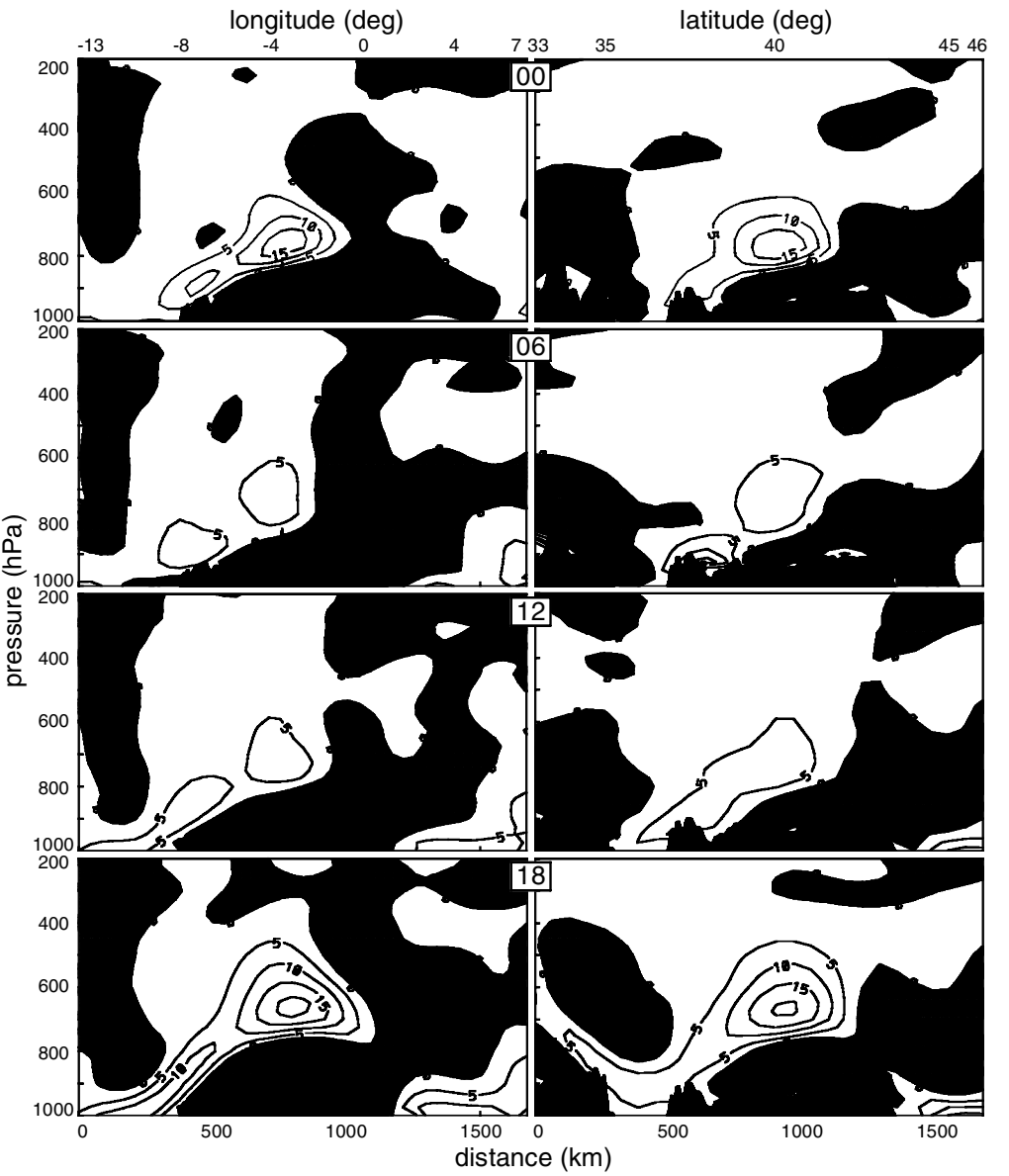


Figure 7. Mean cross-sections of divergence ($10^{-6}$ $s^{-1}$) for July at 00, 06, 12, 18 UTC on thermal-low days: along the parallel of latitude 40.5°N between 13°W and 7°E (left column); along the meridian 4°W between 33°N and 46°N (right column). The averaging period is 1979–1993. The shaded areas indicate convergence.

Iberian thermal low is separate from the Saharan one, at least within the cross-section considered.

A zone of maximum divergence in the zonal cross-section above 800 hPa persists in the same region for the entire day. This divergence is associated with the net mass outflow at this level, which leads to the surface depression. The zone of maximum convergence close to the surface forms in the eastern part of the IP in the morning and shifts towards the centre during the day. The zonal profile of topography shows that the mean slopes towards the interior are larger on the east side of the IP than in

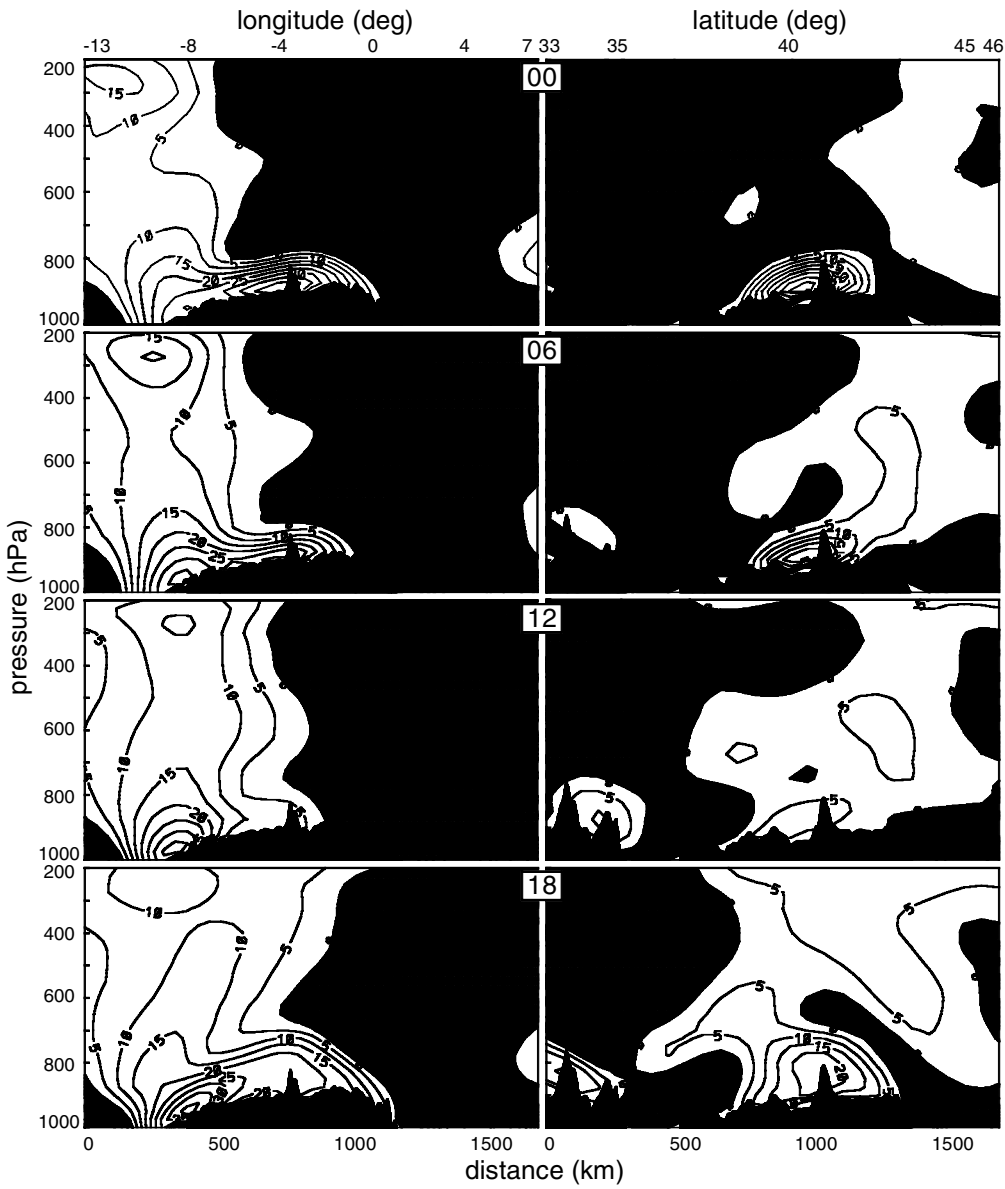


Figure 8. Same as Fig. 7, but for relative vorticity ($10^{-6}$ $s^{-1}$). The shaded areas indicate anticyclonic vorticity.

the west of it. As a result of this, there is a strong inflow from the east. At midnight, as soon as the surface depression weakens, both zones of maxima are found one above the other. In the meridional cross-section, a similar pattern forms where a shift occurs towards the southern end of the convergence maximum: this maximum forms in the afternoon around 18 UTC. It happens also that the shift appears on the side of the peninsula where the major orographic slope is located. This suggests that the zonal and meridional asymmetries can be attributed to the irregular topography of the IP.

Figure 8 indicates that the cyclonic relative vorticity found above the west coast of the IP extends up to the upper troposphere. The low-level behaviour has been discussed

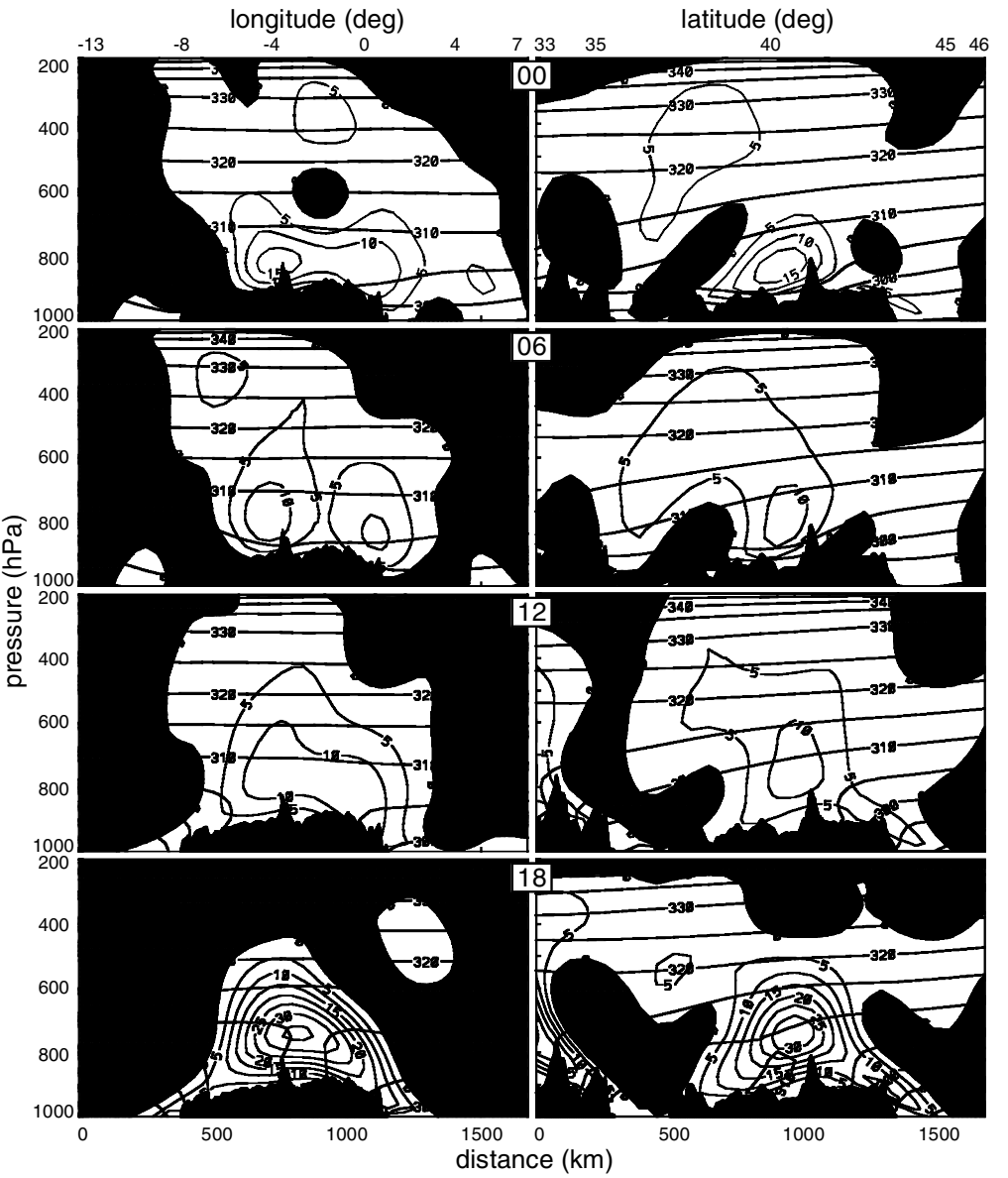


Figure 9. Same as Fig. 7, but for potential temperature (K) (bold lines) and vertical velocity (mm $s^{-1}$) (fine lines). The shaded areas indicate subsidence.

in section 4. The low-level minimum in relative vorticity above the Straits of Gibraltar is apparent up to 800 hPa. The peak hour of maximum cyclonic vorticity is found around 00 UTC in both cross-sections, but the vertical extent is relatively shallow. Figure 8 shows also that the vorticity structure above the IP is irregularly distributed in the horizontal, which makes comparison difficult with vorticity structure obtained from idealized numerical simulations (Rácz and Smith 1999). As noted earlier, orography as well as the non-uniform synoptic environment play an important rôle in modifying the idealized vorticity structure.

The zonal cross-sections in Fig. 9 show the mean vertical velocity and potential temperature. The region with maximum vertical velocity is located directly beneath the zone of strongest divergence and the largest values of more than 3 cm $s^{-1}$ are found during the hour of peak intensity at 18 UTC. Peak vertical velocities of similar magnitude have been reported elsewhere (e.g. Wang 1987). The mean climatological values obtained for the vertical velocity are much smaller than the values obtained in particular events, as has been shown, e.g. by Portela and Castro (1996) where vertical velocities of up to 16 cm $s^{-1}$ were simulated for a July event in 1985. As in other regions with thermal lows, the rate of ascent above the low is noticeably stronger than the surrounding subsidence, by a factor of about three above the IP. In the zonal cross-section, subsidence occurs on both sides of the peninsula. In the meridional cross-section, subsidence prevails above the northern and southern parts of the peninsula at heights above a pressure level about 600 hPa. The existence of significant subsidence between the peninsula and northern Africa is further evidence that the Iberian and Saharan thermal lows are separate systems. On the southern side of the meridional cross-section it is found that the region of ascent over north Africa extends to a much greater height than above the IP, presumably on account of the much larger area and intensity of heating.

The vertical potential-temperature structure shows the typical well-mixed layer above the inner region of the thermal low during the afternoon (Alonso *et al.* 1994). In the zonal cross-section at 18 UTC the top of the mixing layer is found at pressure levels near 700 hPa. A stable stratification is observed above the coastal regions surrounding the IP. Offshore to the west, north and east, the vertical structure of potential temperature remains unchanged during the entire day. Above the surface-based mixed layer, the isentropes behave similarly above land and sea, indicating the relative shallowness of the thermal low that develops over the IP during summer.

## 6. Concluding remarks

In the present paper, statistics of the Iberian thermal low were presented. The major findings of the present study are as follows: During the peak months of June, July and August, a thermal low occurs above the Iberian Peninsula on 35% to 45% of all days. The annual frequency of thermal lows above the IP is about 14% of all days. The most likely location of a thermal low's centre is at 40.5°N and 4.0°W. The hour of peak intensity of the thermal low is around 18 UTC. During the night the low weakens and disappears at around 06 UTC. The dipole layer consists of a surface-based layer of convergence extending to 1500 m agl and a layer of divergence extending to about 5000 m agl. In the central core of the thermal low, ascending mean velocities are typically about 3 cm $s^{-1}$ during the peak hour. A surface-based well-mixed layer extends up to 700 hPa from the late afternoon hours until midnight. The maximum cyclonic vorticity occurs at 00 UTC, some 6 h later than the minimum in the mean-sea-level pressure; this phase shift is of similar magnitude to that found in idealized simulations. It is difficult to interpret the low-level relative-vorticity fields because of their irregular structure which is a result of the irregular orography of the IP and of the strong winds that blow parallel to the west and south coast of the IP.

Rowson and Colucci (1992) reported that thermal lows above south-west North America can produce a moist inflow from coastal regions. The IP is surrounded mostly by sea. The inland penetration of moist sea air is irregular over the peninsula. From the south-east, east and north the air can penetrate more than 200 km inland, sometimes through mountain passes, but from the south there is little detectable inflow, except

through the Guadalquivir river valley. In general, there is no significant moisture transport towards the semi-arid centre of the IP where most thermal lows are located. The reasons for this are that the distance of 300 to 400 km from the coast is too large, the inflow is relatively weak and the strong low-tropospheric vertical mixing transports dry air from aloft down to the surface. Therefore, this study gives no statistics on the moisture structure.

It is well-known that the summer surface heating over the IP generally favours the development of a thermal circulation. However, only on a limited number of days are the heating conditions strong enough to allow the generation of a thermal low. Besides this, the synoptic-scale environment might play a determining role in forcing or suppressing the generation of a thermal low. It would be interesting to determine if there are particular synoptic conditions which favour the generation of a thermal low and also which ones do not. However, this can be studied only with numerical simulations.

Most studies indicate that the uppermost level of a thermal low's impact is not higher than about 5000 m; for the much stronger thermal low observed above Australia, the top influence level might be considerably higher. Wang (1987) reported depths of up to 10 km above the Tibetan Plateau. For the very prominent thermal depression above the Arabian Peninsula, Smith (1986b) found that the subsidence layer extends vertically up to 200 hPa. For both examples the thermal low has an impact on the entire troposphere up to the tropopause. Yet it is not clear if there is an influence of the shallow Iberian thermal low at higher altitudes. In a preliminary study, which is based on ozone column data and tropopause data taken from radiosonde and derived from ERA data, statistics above the main lifting core of the Iberian thermal depression were determined. The result is that on summer days with a thermal low the tropopause pressure (height) is decreased (increased) by about 5 hPa (200 m) and correspondingly the total ozone column is decreased by about 7 DU. These values are statistically significant whereas the estimated vertical velocity at tropopause level ($\approx$0.5 mm $s^{-1}$) were statistically insignificant. Recent work indicates that there is a summer minimum in total ozone above the IP, particularly during July (Cuevas *et al.* 2001). Because July is the peak month for the occurrence of thermal lows it is suggestive that the low-tropospheric thermal low might influence upper-tropospheric structure and the behaviour of the tropopause. The given statistics seem to corroborate this or at least do not exclude this possibility.

## Acknowledgements

The ERA data was kindly provided by the ECMWF within the special project entitled 'The climatology of the global tropopause'. Adelaida Portela (Universidad Europea, Madrid) is thanked for discussing thermal-low criteria with us. We are very grateful also to Roger K. Smith (University of Munich) for his thoughtful critique of the original manuscript and for improving the English of the text. Preliminary work towards this study was performed by the first author (K. P. Hoinka) during a two-months stay at the University Complutense in Madrid in 1993.

## References

Alonso, S., Portela, A. and Ramis, C. 1994 First considerations on the structure and development of the Iberian thermal low-pressure system. *Ann. Geophys.*, **12,** 457–468

Blake, D. W., Krishnamurti, T. N., Low-Nam, S.V. and Fein, J. S. 1983 Heat low over the Saudi Arabian desert during May 1979 (summer MONEX). *Mon. Weather Rev.*, **111,** 1759–1775

Burger, A. and Ekhart, E. 1937 Über die tägliche Zirkulation der Atmosphäre im Bereich der Alpen. *Gerl. Beitr. Geophys.*, **49,** 341–367

Campins, J., Genovés, A., Jansá, A., Guijarro, J. A. and Ramis, C. 2000 A catalogue and a classification of surface cyclones for the western Mediterranean. *Int. J. Climatol.*, **20,** 969–984

Chang, J. H. 1972 *Atmospheric circulation systems and climates*. Oriental Publishing Company, Honolulu, HW

Cuevas, E., Gil, M., Rodriguez, J., Navarro, M. and Hoinka, K. P. 2001 Sea–land total ozone differences from TOMS: The GHOST effect. *J. Geophys. Res.*, **106 D21,** 27745–27755

Font, I. 1983 *Climatología de España y Portugal*. Instituto Nacional de Meteorología. Madrid.

Gaertner, M. A., Fernández, C. and Castro, M. 1993 A two-dimensional simulation of the Iberian summer thermal low. *Mon. Weather Rev.*, **121,** 2740–2756

Gaertner, M. A., Christensen, O. B., Prego, J. A., Polcher, J., Gallardo, C. and Castro, M. 2001 The impact of deforestation on the hydrological cycle in the Western Mediterranean: An ensemble study with two regional climate models. *Clim. Dyn.*, **17,** 857–873

Gibson, R., Kållberg, P., Uppala, S., Hernandez, A., Nomura, A. and Serrano, E. 1997 ERA Description. ECMWF-ReAnalysis project Report Series No. 1. European Centre for Medium-Range Weather Forecasts, Shinfield Park, Reading, Berkshire RG2 9AX, UK

Griffiths, J. F. and Soliman, K. H. 1972 'The northern desert'. Pp. 75–110 in *World survey of climatology*, Vol. 10, *Climates of Africa*. Ed. J. F. Griffiths. Elsevier, Amsterdam

Hernandez, A. 1997 'A potential vorticity based statistical study on cut-off lows over southwestern Europe'. Pp. 343–348 in Proceedings of international symposium on cyclones and hazardous weather in the Mediterranean, 14–17 April 1997, Palma de Mallorca, Spain, INM/WMO

Hoinka, K. P. and Rösler, F. 1987 The surface layer on the leeside of the Alps during foehn. *Meteorol. Atmos. Phys.*, **37,** 245–258

Hoinka, K. P. and Seco, J. 1991 Sobre frentes fríos en la Península Ibérica. *Rev. de Geofísica*, **47,** 149–168

Junning, L., Zhengan, Q. and Fumin, S. 1986 'An investigation of the summer lows over the Qinghai-Xizang plateau'. Pp. 369–386 in Proceedings of the international symposium on Qinghai-Xizang Plateau and mountain meteorology, 20–24 March, Beijing. American Meteorological Society, 45 Beacon Street, Boston MA02108-3693, USA

Lautensach, H. 1964 *Die iberische Halbinsel*. Keysersche Verlagsbuchhandlung, Munich, Germany

Leslie, L. M. 1980 Numerical modelling of the summer heat low over Australia. *J. Appl. Meteorol.*, **19,** 381–387

Linés, A. 1970 The climates of the Iberian Peninsula. Pp. 195–226 in *Climates of Northern and Western Europe*. Ed. C. C. Wallén. World Meteorological Organization, Geneva

1981 Pertubaciones típicas que afectan a la Península Ibérica y precipitaciones asociadas. Publicación No. A-80, Instituto Nacional de Meteorología, Madrid

Millán, M., Artiano, B., Alonso, S., Navazo, M. and Castro M. 1991 The effect of mesoscale lows on regional and long-range atmospheric transport in western Mediterranean area. *Atmos. Environ.*, **25A,** 949–963

Orlanski, I. 1975 A rational subdivision of scales for atmospheric processes. *Bull. Am. Meteorol. Soc.*, **56,** 527–530

Portela, A. and Castro, M. 1991 Primera aproximación a una climatología de las depresiones térmicas en la Península Ibérica. *Rev. de Geofísica*, **47,** 205–215

1996 Summer thermal lows in the Iberian Peninsula: A three-dimensional simulation. *Q. J. R. Meteorol. Soc.*, **122,** 1–22

Rácz, Z. and Smith, R. K. 1999 The dynamics of heat lows. *Q. J. R. Meteorol. Soc.*, **125,** 225–252

Ramage, C. S. 1971 *Monsoon Meteorology*, Academic Press, N.Y.

Reichmann, Z. and Smith, R. K. 2003 Terrain influences on the dynamics of heat lows. *Q. J. R. Meteorol. Soc.* (in press)

Rowson, D. R. and Colucci, S. J. 1992 Synoptic climatology of thermal low-pressure systems over the south-western north America. *Int. J. Climatol.*, **12,** 529–545

Scherhag, R. 1936 Synoptische Untersuchung der täglichen Luftdruckschwankung über Mitteleuropa. *Ann. Hydr. Marit. Meteorol.*, **64,** 291–294

Smith, E. A. 1986a The structure of the Arabian heat low. Part I: Surface energy budget. *Mon. Weather Rev.*, **114,** 1067–1083

1986b The structure of the Arabian heat low. Part II: Bulk tropospheric heat budget and implications. *Mon. Weather Rev.*, **114,** 1084–1102

Smith, R. K., Reeder, M. J, Tapper, N. J and Christie, D. R. 1995 Central Australian cold fronts. *Mon. Weather Rev.*, **123,** 16–38

Soler, A. M. and Hernandez, E. 1977 Situaciones meteorológicas locales típicas: Descripción y frecuencia de las mismas. *Rev. de Geoftsica*, **36,** 111–122

Wang, B. 1987 The development mechanism for Tibetan Plateau warm vortices. *J. Atmos. Sci.*, **44,** 2978–2994

Whitehead, J. B. 1981 Mesoscale thermal lows in Tasmania. *Weather*, **36,** 180–183